Electronic Supplementary Material (ESI) for RSC Advances
This journal is © The Royal Society of Chemistry 2013

Supporting Information

Synthesis of $FeTiO_3$ nanosheets with {0001} facets exposed: Enhanced electrochemical performance and catalytic activity

Xiang-Feng Guan, Jing Zheng, Ming-Lei Zhao, Li-Ping Li and Guang-She Li*

State Key laboratory of Structural Chemistry, Fujian Institute of Research on the Structure of Matter, Chinese Academy of Sciences, Fuzhou 350002,P. R. China.

*E-mail: guangshe@fjirsm.ac.cn; Fax: (+86)-591-83702122, Tel: (+86)-591-83702122.

Experimental details

Chemicals: Tetrabutylammonium hydroxide (TBAH, 10% aqueous solution, Sinopharm Chemical Reagent Co., Ltd.), titanium isopropoxide (TTIP, Aldrich Chemical Co., 97%), $FeSO_4 \cdot 7H_2O$ (Sinopharm Chemical Reagent Co., Ltd., 99%), KOH (Sinopharm Chemical Reagent Co., Ltd., 99%), deionized water. All reagents were used as received without further purification.

Evaluation of pseudocapacitance property: Electrochemical characterization was done by cyclic voltammetry (CV) and by galvanostatic charging-discharging using a three-electrode mode in a 1 M KOH aqueous solution. The working electrodes were prepared by mixing the as-prepared $FeTiO_3$ (80 wt%), acetylene black (15 wt%) and polyvinylidene fluoride (PVDF, 5 wt%) in N-methyl-2-pyrrolidone (NMP). After that, the mixture was coated onto the nickel foam (1 cm^2) to form the electrode layer by drying at 100 ^oC at vacuum for around 6 hours. The reference electrode and counter electrode were Hg/HgO electrode and platinum foil, respectively. Typical

This journal is © The Royal Society of Chemistry 2013

CV curves were measured between -0.4-1.2 V. The discharge specific capacitance is calculated from the discharge curves using the following formula, $C = I \cdot \Delta t / (\Delta V \cdot m)$, where I (A), Δt (s), m (g), and ΔV (V) are the discharge current, discharge time consumed in the potential range of ΔV, mass of the active materials, and the potential windows, respectively.[6]

S1

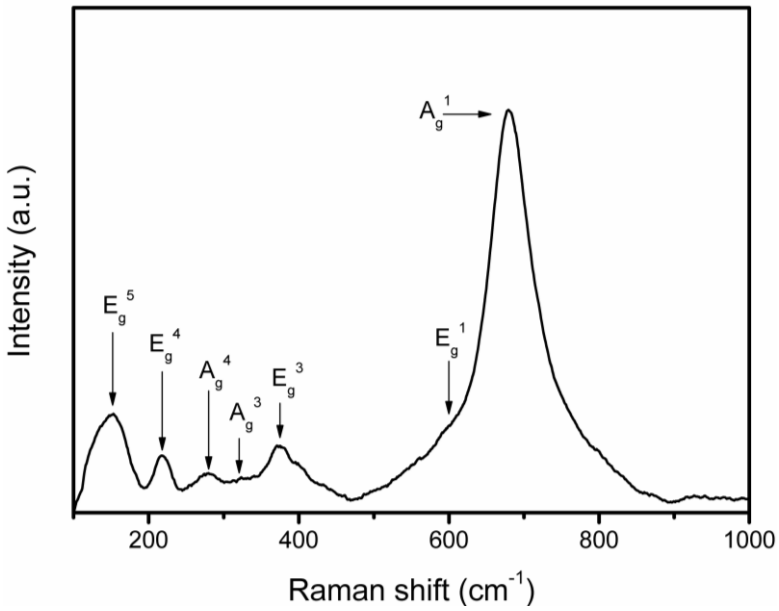

Figure S1 Raman spectrum of the as-prepared $FeTiO_3$ nanosheets

Raman spectrum of the as-prepared $FeTiO_3$ nanosheets is shown in Figure S1. In the case of Raman analysis, group theory analysis of ilmenite $FeTiO_3$ predicts ten Raman active lattice vibration modes, which are assigned based on ionic substitution: A_g^1 and E_g^1 mode to Ti-O stretching motions; A_g^2, A_g^3, E_g^2 and E_g^3 to O-Ti-O bending motions; A_g^4 and E_g^4 to translations of the TiO_6 octahedra against Fe^{2+} cations; A_g^5 and E_g^5 to translations of the Fe^{2+} cation against the oxygen framework.[3] Although all the ten vibration modes were not observed in the Figure S1, representative Raman signals of 151, 217, 280, 320, 374, 598, and 690 cm^{-1}, which is

This journal is © The Royal Society of Chemistry 2013

corresponding to vibration modes of A_g^1, E_g^1, E_g^3, A_g^3, A_g^4, E_g^4, and E_g^5, respectively, are observed to confirm the ilmenite $FeTiO_3$ structure for comparison with previous reports.[4]

S2

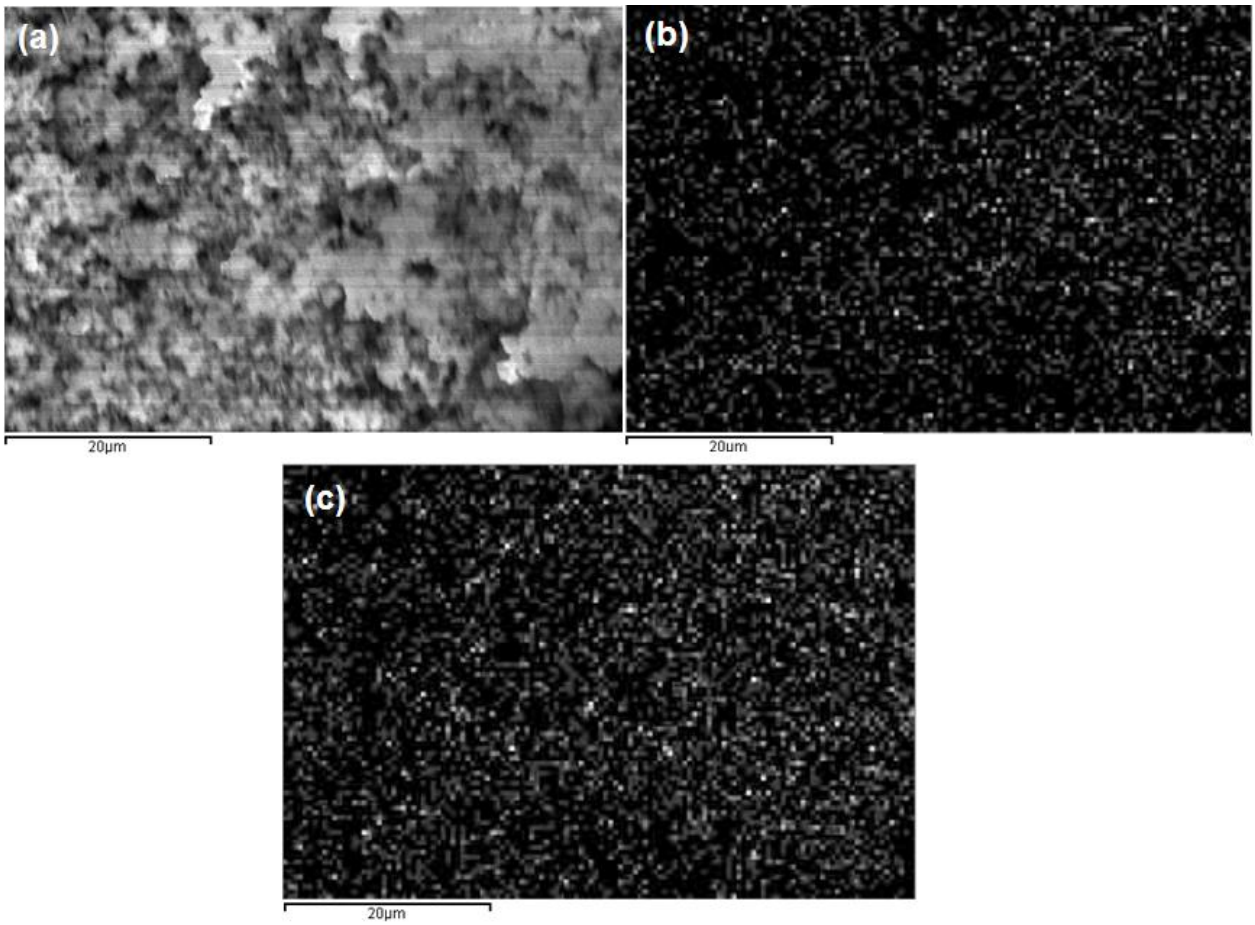

Figure S2 SEM image (a) and X-ray mapping of Fe (b) and Ti (c) of as-prepared $FeTiO_3$ nanosheets

In order to confirm the chemical composition of as-prepared $FeTiO_3$ nanosheets, elemental mapping and quantitative analysis were performed using EDS. As indicated by Figure S2, both elements Fe and Ti are identified and homogeneously distributed in the sample. The results of

This journal is © The Royal Society of Chemistry 2013

quantitative elemental analysis show that the atomic ratio of Fe and Ti is 10.53:11.97, closer to the stoichiometry of $FeTiO_3$. These results further verified the formation of $FeTiO_3$ nanosheets.

S3

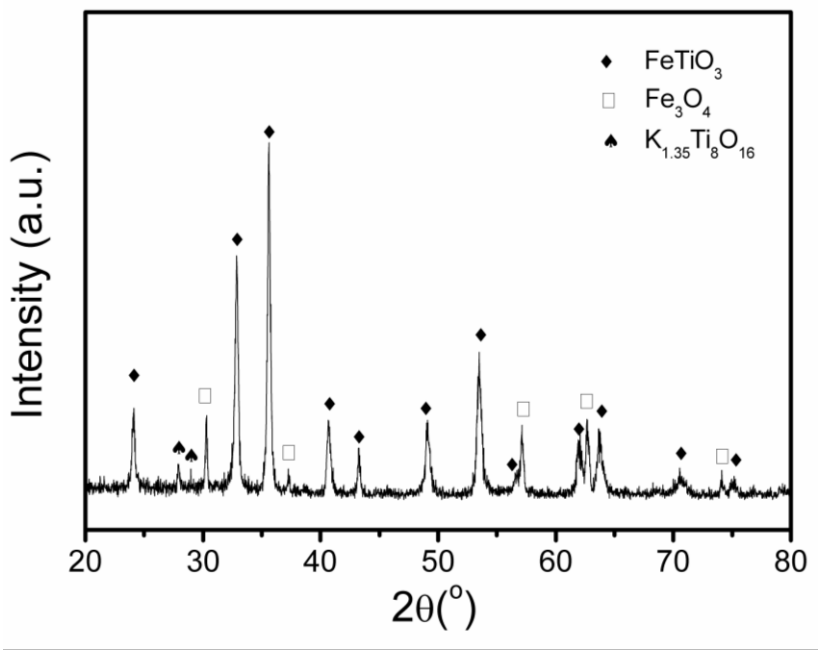

Figure S3 XRD pattern of the products prepared without TBAH. ($K_{1.35}Ti_8O_{16}$ JCPDS 47-0690; Fe_3O_4 JCPDS 19-0629)

This journal is © The Royal Society of Chemistry 2013

S4

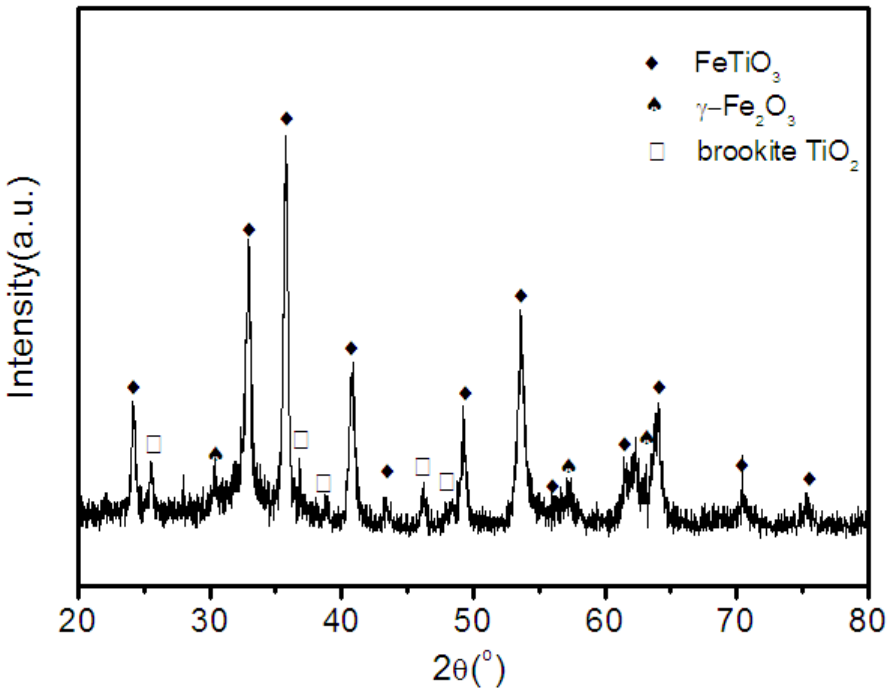

Figure S4 XRD pattern of the products prepared in the solution with pH value=12. (Brookite TiO_2 JCPDS 29-1360)

S5

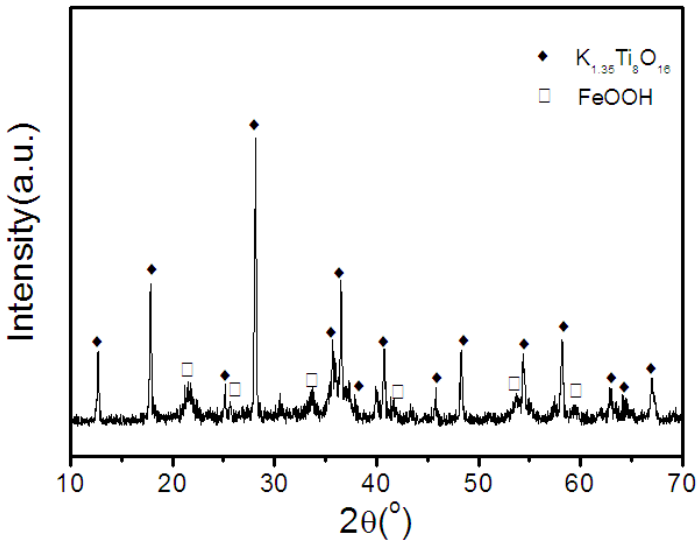

Figure S5 XRD pattern of the products prepared by stirring the precursor for 60 min (FeOOH JCPDS 46-1436)

This journal is © The Royal Society of Chemistry 2013

S6

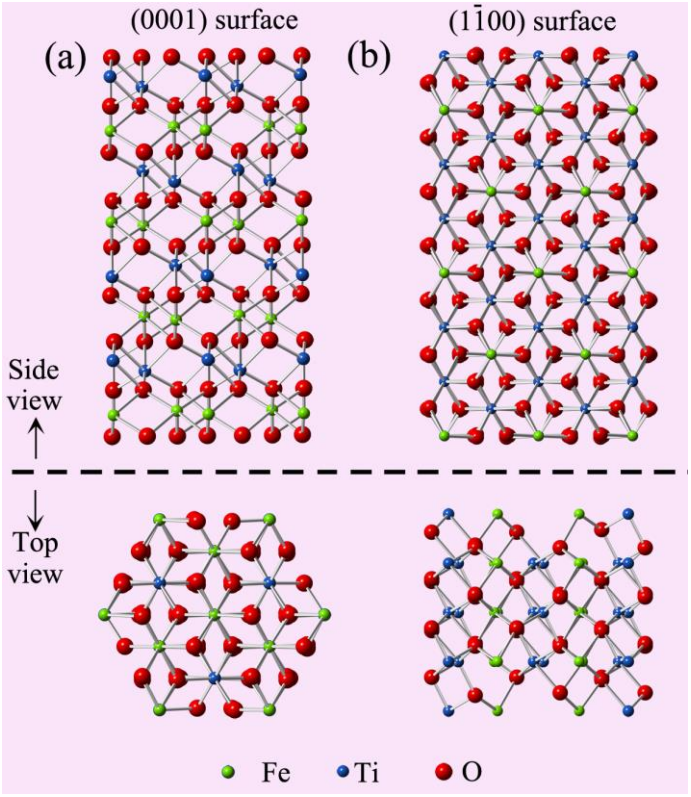

Figure S6 Side and top views of the relaxed: (a) (0001) and (b) (1$\bar{1}$00) surfaces of $FeTiO_3$ nanosheets. The growth slices are demarcated by dotted-dashed lines.

S7 Calculation of surface energy

The CASTEP method[1] was used to calculate the crystal energy and the surface energy. The unit cell model of the $FeTiO_3$ crystal was set up according to ICSD 30669, a=5.088 nm and c=14.093 nm. The surface models of (0001) and (1$\bar{1}$00) planes were constructed with about 7-9 layers of atoms cleaved on the planes before a vacuum slab of 10.00 Å in thickness was built on the corresponding crystal surface. The energy of each plane was calculated using the generalized gradient approximation (GGA) with the gradient corrected functional Perdew-Burke-Ernzerhof (PBE). The ultrasoft pseudopotentials (USP) were applied with a plane wave energy cutoff of 340 eV. The 6 × 6 × 1, and 3 × 5 × 1 k points were used for the Brillouin zone of models of (1$\bar{1}$00) and (0001), respectively. The other parameters were set as default. The self-consistent

This journal is © The Royal Society of Chemistry 2013

calculations are converged only when the total energy converges to less than 10^{-6} eV/atom. The surface energy is achieved through the following formula: [2]

$$E_{sur} = (E_{tol} - nE_{cell}) / S$$

E_{sur} is the surface energy of the $FeTiO_3$ crystal, E_{tol} is the total energy of the surface model, E_{cell} is the energy of one unit cell of the bulk $FeTiO_3$, n refers to the number of unit cell in the established model, and S is the surface area of the calculation model. The calculation results are listed in Table 1.

Table 1 Surface energy (E_{sur}) of different $FeTiO_3$ crystal surfaces

Model plane	(0001)	$(10\bar{1}0)$	$(01\bar{1}0)$	$(1\bar{1}00)$
E_{sur} (J/m^2)	22.0506	1.9559		

S8

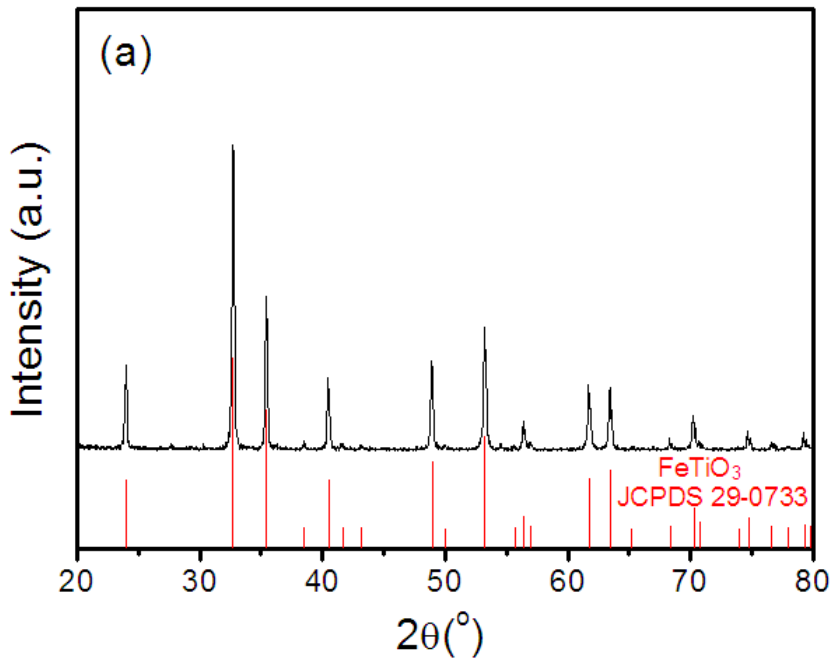

This journal is © The Royal Society of Chemistry 2013

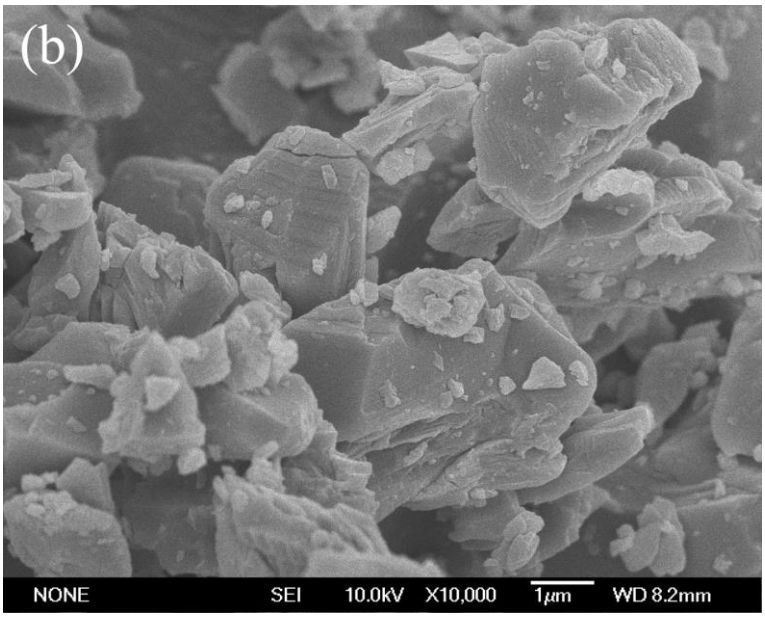

Figure S8 XRD pattern (a) and SEM image (b) of commercial irregular $FeTiO_3$

S9

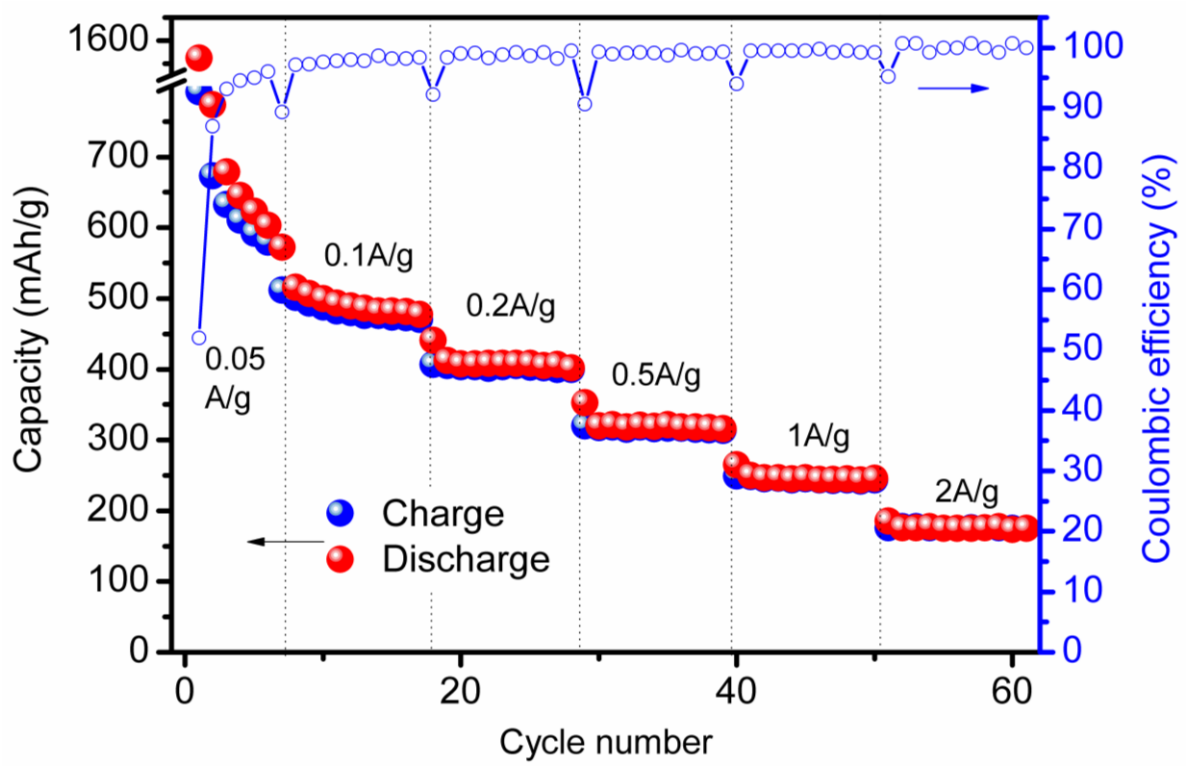

Figure S9 Rate capabilities of $FeTiO_3$ nanosheets electrode at different current rates.

This journal is © The Royal Society of Chemistry 2013

Considering that the rate capability is also very important for practical applications, the cycling behavior of $FeTiO_3$ nanosheets electrode at different current densities was evaluated. Figure S9 shows the rate capability of the $FeTiO_3$ nanosheets electrode for current density up to 2 A/g. The cell was first cycled at a current density of 0.1 A/g, and after every 11 cycles was gradually increased in stages to 2 A/g. At current densities of 0.05, 0.1, 0.2, 0.5, 1, and 2 A/g, the $FeTiO_3$ nanosheets delivered specific capacities of 560, 450, 400, 310, 250, 180 mAh g^{-1} respectively, while maintaining an excellent Coulombic efficiency of over 99 %.

S10

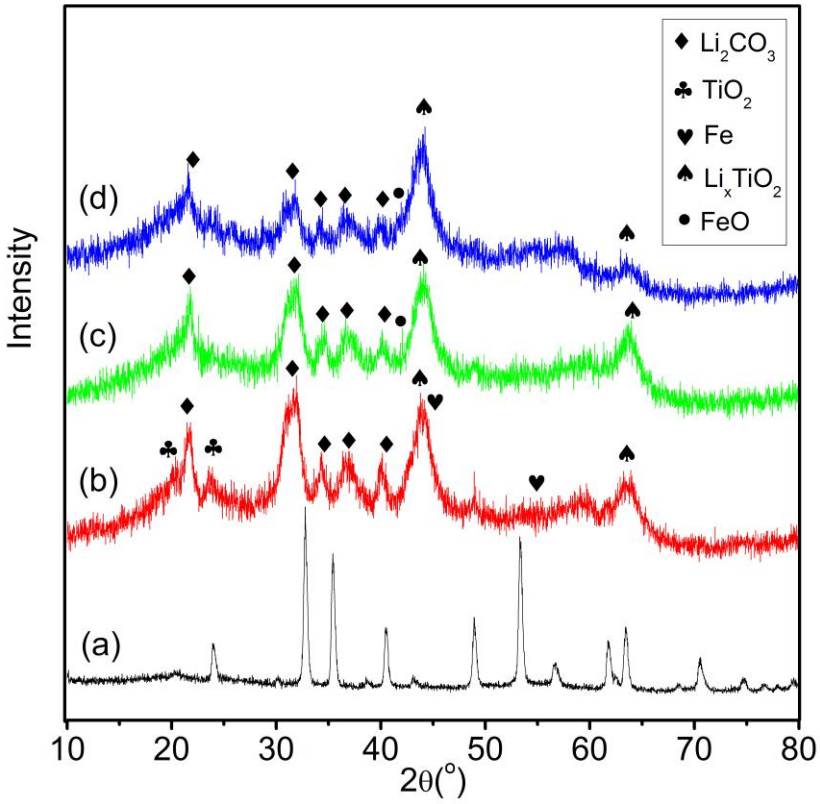

Figure S10 XRD patterns of $FeTiO_3$ electrode: (a) as-prepared; (b) first discharged to 0.01 V; (c) first discharged to 1 V; (d) first charged to 3 V. (Li_2CO_3 —PDF 87-0729; TiO_2 —PDF 70-2556; Fe —PDF 65-4150; Li_xTiO_2 —PDF 16-0223; FeO —PDF 75-1550)

This journal is © The Royal Society of Chemistry 2013

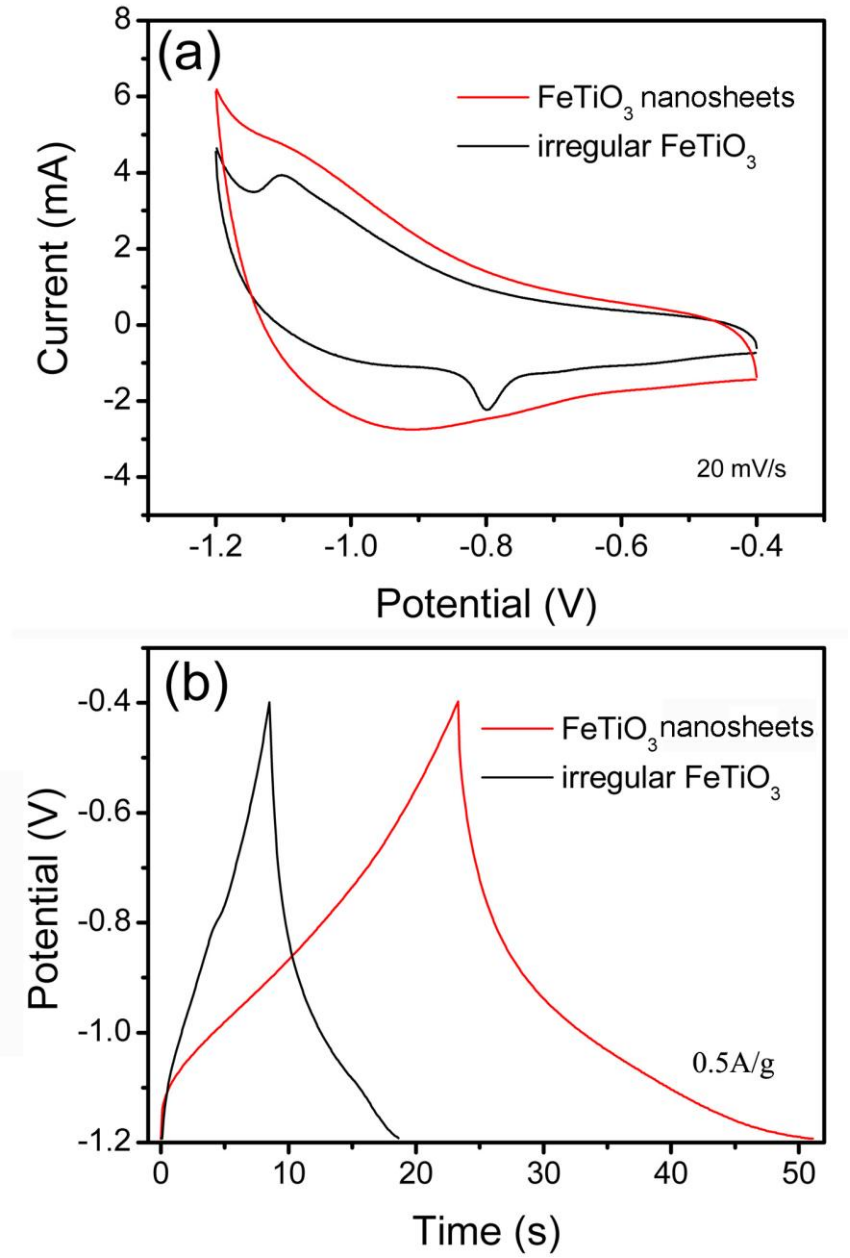

Figure S11 (a) Cyclic voltammetry curves and (b) charge-discharge profiles of the $FeTiO_3$ nanosheets and irregular $FeTiO_3$

Besides the lithium storage property, the pseudocapacitive behavior of $FeTiO_3$ nanosheets was also measured, since $FeTiO_3$ incorporating two metal cations may provide capacitances over larger potential windows and involve redox chemical reactions over Fe^{2+} and Ti^{4+}.[5] Accordingly, the pseudocapacitive property of the $FeTiO_3$ nanosheets were evaluated by CV and

This journal is © The Royal Society of Chemistry 2013

charge-discharge measurement in 1 M KOH aqueous solutions. For a direct comparison, the CV curves and charge-discharge profiles under the same scan rate of irregular $FeTiO_3$ are depicted in Figure S11 (a) and (b), respectively. As shown in Figure S11 (a), at a scan rate of 20 mV/s, the CV curves of $FeTiO_3$ nanosheets are closer to the elliptical ones while those for irregular shows a pair of distinct redox peaks. The area enclosed by the CV curve of $FeTiO_3$ nanosheets is obviously larger than that for irregular $FeTiO_3$. These indicate that $FeTiO_3$ nanosheets exhibit larger capacitance than irregular $FeTiO_3$. The capacitance improvement can also be seen from the charge-discharge curves, as shown in Figure S11 (b). At the current density of 0.5 A/g, the capacitance measured for irregular $FeTiO_3$ is 8.2 F/g, while the capacitance for $FeTiO_3$ increased to 17.6 F/g, even though the capacitance for both samples deserve more work to improve. An improved electrochemical behavior of the $FeTiO_3$ nanosheets may be attributed to their small particle size and unique 2D nanostructure.

Reference

1. M. D. Segall, P. J. D. Lindan, M. J. Probert, C. J. Pickard, P. J. Hasnip, S. J. Clark, and M. C. Payne, *J. Phys. Condens. Matter, 2002,* 14, 2717.
2. Y. Wang, J. Chen, P. Wang, L. Chen, Y. B. Chen and L. M. Wu, *J. Phys. Chem. C*, 2009, **113**, 16009.
3. X. Wu, S. Qin and L. Dubrovinsky, *Geoscience Frontiers*, 2011, **2**, 107.
4. Y. K. Sharma, M. Kharkwal, S. Uma and R. Nagarajan, *Ploy*hedron, 2009, **28**, 579.
5. T. Tao, A. M. Glushenkov, H. W. Liu, Z. W. Liu, X. J. J. Dai, H. Chen, S. P. Ringer and Y. Chen, *J. Phys. Chem. C.*, 2011, **115**, 17297.
6. J. Yan, E. Khoo, A. Sumboja and P. S. Lee, *ACS Nano*, 2010, **4**, 4247.